Published in final edited form as:
Anal Chem. 2011 April 1; 83(7): 2748–2753. doi:10.1021/ac103374x.

Nine Orders of Magnitude Dynamic Range: Picomolar to Millimolar Concentration Measurement in Capillary Electrophoresis with Laser Induced Fluorescence Detection Employing Cascaded Avalanche Photodiode Photon Counters

Oluwatosin O. Dada[a], **David C. Essaka**[a,b], **Ole Hindsgaul**[c], **Monica M. Palcic**[c], **Jillian Prendergast**[d], **Ronald L. Schnaar**[d], and **Norman J. Dovichi**[a]

[a]Department of Chemistry and Biochemistry, University of Notre Dame, Notre Dame, IN. 46556 USA

[b]Department of Chemistry, University of Washington, Box 351700, Seattle, WA. 98195 USA

[c]Carlsberg Laboratory, Gamle Carlsberg Vej 10, DK-2500, Valby Copenhagen Denmark

[d]Departments of Pharmacology and Neuroscience, The Johns Hopkins School of Medicine, 725 N. Wolfe Street, Baltimore, MD 21205 USA

Abstract

The dynamic range of capillary electrophoresis analysis is ultimately limited by molecular shot noise at low concentrations and by concentration-induced band broadening at high concentrations. We report a system that approaches these fundamental limits. A laser-induced fluorescence detector is reported that employs a cascade of four fiber-optic beam-splitters connected in series to generate a primary signal and four attenuated signals, each monitored by a single-photon counting avalanche photodiode. Appropriate scaling of the signals from the five photodiodes produces a linear optical calibration curve for 5-carboxyl-tetramethylrhodamine from the concentration detection limit of 1 pM to the upper limit of 1 mM. Mass detection limits are 120 yoctomoles (70 molecules) injected into the instrument. The very-wide dynamic range instrument was used to study the metabolic products of the fluorescently labeled glycosphingolipid GM1-TMR produced by single cells isolated from the rat cerebellum.

INTRODUCTION

It is sometimes desirable to simultaneously monitor the abundances of both a trace component and a major component that is present at much higher concentration. For example, in single-cell enzymatic studies, metabolic products may be at much lower abundance than the substrate.[1] There are two serious challenges involved in such measurements. First, it is necessary to discriminate the signal generated by the trace component from that generated by the major component. Second, it is necessary to employ a detector with a requisite wide dynamic range for the components. Real-time polymerase chain reaction is an example of a method that provides such discrimination power and high dynamic range for the analysis of oligonucleotides.[2]

Correspondence to: Norman J. Dovichi.

Characterization of other biological analytes across a wide dynamic range is more challenging. Fluorogenic reagents provide an approach to the characterization of selected enzymatic transformations.[3] In these cases, the enzyme converts the weakly fluorescent substrate into a highly fluorescent product. Such measurements are limited to those enzymatic reactions where a fluorogenic reagent is available, and become extremely difficult when characterizing an enzymatic cascade, where a substrate undergoes sequential biosynthetic steps to create a product.

The use of chromatographic or electrophoretic separations provides a more universal approach to the discrimination of trace level product from major component. Such analyses must address the real-world reality of separations. Minor deviations from a linear isotherm, minute amounts of extra-column band broadening, and incomplete approach to equilibrium can lead to tailing and fronting, which cause deviations from a Gaussian peak shape that obliterate the resolution of the components. An equal or greater challenge is provided by trace level impurities that can interfere in the analysis. Preparation of reagents with purity at the part-per-billion level requires heroic efforts. As one useful tool, we have found photobleaching using inexpensive light-emitting diodes reduces the reagent blank in laser-induced fluorescence experiments.[4]

Wide dynamic range detection is also challenging. State of the art absorbance detectors are limited to five orders of magnitude dynamic range by instabilities in the source intensity.[5] Fluorescence and light scattering can provide higher dynamic range. In these cases, the detection limit is determined by shot-noise in the detector dark current, shot-noise in the background signal, or noise in the background signal that is proportional to fluctuations in the source intensity.[6] The detector ultimately saturates at high fluorescence signals. For example, conventional fluorescence detectors are often limited by the dynamic range of the instrument's analog-to-digital converter. An instrument with a 16-bit converter can generate four and a half orders of magnitude dynamic range, although signal averaging can extend the dynamic range.

Photon counting can provide improved performance at low signal levels by discriminating against some of the dark current inherent in the detector.[7] Such improvements are only significant when the instrument's blank signal is lower than the dark current. Unfortunately, the background signal generated by weak Raman scatter or fluorescent impurities often is often much higher than the detector dark signal, in which case photon counting does not significantly improve detection limits. Instead, photon counting can extend the dynamic range of the measurement because the counts can be accumulated to arbitrarily large values.

For CW excitation, the detector's dead time limits the dynamic range of photon counters.[8–10] This dead time is due to the transit time of the current pulse through the dynode chain of a photomultiplier tube or to the quenching time of an avalanche photodiode. A second photon that arrives during the dead time will not be detected. If the detector does not respond to the subsequent photon, then the detector's response will monotonically approach a saturating value at high intensity. In a paralizable detector, the dead time is reset upon arrival of a second photon. In this case, the detector's response reaches a maximum and then decreases to zero at higher intensities. In most cases, the dynamic range of a fluorescence instrument based on a photon counter is limited to four orders of magnitude. A variety of models have been constructed to linearize the response of the photon counter, which can perhaps extend the dynamic range by an order of magnitude.[8–10]

The situation is different for pulsed excitation. Gustafson reported the use of multilevel discrimination to correct for pulse overlap in photon counting with pulsed laser excitation and photomultiplier detection.[11] Kissick recently reported a similar system that employed

software-based discriminators to produce six orders of magnitude dynamic range in optical intensity.[12] Both cases required subnanosecond pulsed excitation, which adds to the instrument's expense. Neither case evaluated an analytical detection limit.

We previously reported a laser-induced fluorescence detector that employed a cascade of two beam-splitters and three photodiodes to generate six orders of magnitude dynamic range for electrophoretic detection.[13] In this approach, the collected light in a fluorescence instrument was split by fiber-optic devices and directed to a set of avalanche photodiodes. The train of photodiodes simultaneously measured successively more attenuated fluorescence intensity. The signals were combined so that the highest sensitivity detector reported the lowest intensity signals, the intermediate sensitivity detector reported intermediate intensity signals, and the lowest sensitivity detector reported the highest intensity signals. Since only the most sensitive detector was used to measure the lowest intensity signal, there was no additive noise from combining signals from several detectors.

This system has several advantages. The design is robust because it operates with rugged avalanche photodiodes and rugged fiber optical components that are designed for the communication industry; the dynamic range of detection can be extended to arbitrarily high values; and the detector employs an inexpensive and reliable continuous wave laser.

In this paper, we extend the dynamic range by three orders of magnitude, so that and the lower limit approaches molecular shot noise. This thousand-fold increase in dynamic range was accomplished with two addition fiber optic beam splitters and two avalanche photodiodes. We apply the instrument to metabolic cytometry analysis of glycolipid metabolism in primary rat cerebellum cells.

Materials and Methods

Capillary electrophoresis

The laser-induced fluorescence/ capillary electrophoresis system is similar to others reported by our group.[13–18] For 5-carboxyl-tetramethylrhodamine (TAMRA) measurements, a 33 cm long, 31 μm ID, and 150 μm OD bare fused silica capillary is used. The separation running buffer is 10 mM borate and the separation is performed at 20 kV. Injection is for 1 s at 1 kV. Counts are recorded at 50 Hz. The instrument is equipped with a post-column sheath-flow cuvette for fluorescence detection. The separation buffer and the capillary length are different for single cell measurements. The capillary for single cell measurement is 30-μm ID and 38 cm long. The single cell separation buffer is composed of 10 mM sodium tetraborate, 35 mM sodium deoxycholate, and 5 mM methyl-β-cyclodextrin.

High Dynamic Range CE-LIF Instrument

The optical design of the high-dynamic range system is similar to the one previously reported, Figure 1.[13] Excitation is provided with a 10 mW diode-pumped solid-state laser beam at 532 nm that is focused in a sheath-flow cuvette.[14,15] Fluorescence is collected by a 0.70 NA microscope objective, passed through a 580 DF40 bandpass filter, and imaged onto a GRIN-lens coupled fiber optic. The fiber optic is coupled to a train of four fiber optics beam-splitters and five avalanche photodiode detectors (APDs).

We employ a train of four cascaded fiber-optic beam-splitters to divide the fluorescence into five channels; one channel retains most of the original intensity and the subsequent channels present attenuated versions. The beam-splitters (Timbercon, Inc.) have a nominal 99:1 split ratio at 850 ± 40 nm. The split ratio degrades at the 580 nm emission wavelength of the fluorescence. The first splitter generates a split ratio of ~27:1 and the others generate a split ratio of ~6:1. The splitters are placed in series, such that the less intense output of one

splitter is directed to the input of the next splitter. The intense output of each splitter, along with the less intense output of the last splitter, is connected to a single photon counting avalanche photodiode. PerkinElmer SPCM single photon counting modules are employed in the experiment; all have nominal dead time of 55 ns. The splitters and associated optical fibers are covered with an opaque plastic sheet to eliminate background signal due to room light that leaks through the fiber's cladding.

The outputs of the photodiodes are digitized at 50 Hz by counters (National Instruments) with a Labview program in a PC. The data are then processed on a Macintosh computer using Matlab. Data are first corrected for detector dead time, treated with a five point median filter, and then convoluted with a 44-point wide Gaussian function with 5-point (100 ms) standard deviation. The Matlab routine *cftool* is used to fit a Gaussian function to the TAMRA peak; peak area is estimated as $\sqrt{2\pi}$ * peak amplitude * peak standard deviation.

The beam-splitters show some wavelength dependence. Since the background signal has different spectrum than the TAMRA fluorescence, the two components have different scaling factors. In addition, dark counts should not be used when scaling. To deal with these issues, we first subtract the background from each photodiode signal. Then, the analyte signals are multiplied by a factor that accounts for the attenuation experienced by each photodiode, the signals are combined to make a smooth scaled electropherogram, and finally the first diode's background signal is added back to the data. The supporting information section of this paper presents the M-file used to scale the corrected data.

Single Cell Analysis

Collection and culture of cells from the rat cerebellum was adapted from an established protocol.[19] Cerebella were dissected from postnatal day 5–6 rats, the meninges were removed and the brain tissue was dissociated with a papain dissociation kit (Worthington) using the supplier's protocol. Briefly, freshly isolated brain tissue was bathed in a solution of papain and DNase for 30 min at 37°C, then cells were dissociated by trituration with a fire-polished glass pipette. Dissociated cells were collected by centrifugation (10 min, 240 × g), re-suspended in containing solution of ovomucoid papain inhibitor, and re-collected by centrifugation. Cells were finally re-suspended in serum-free growth medium at 1 million cells/mL and plated at 2 mL per 35 mm tissue culture dish. Cells were cultured at 37°C in a humidified 5% CO_2 atmosphere for 11 days before addition of the fluorescent lipid. Cells were cultured for 14 h in medium containing 5 μM tetramethylrhodamine labeled GM1 (GM1-TMR),[20] washed with fresh medium without GM1-TMR, then incubated for 45 min with 2.5 μM of CellTracker CMFDA (Invitrogen). The medium was replaced with fresh medium containing neither GM1-TMR nor CMFDA, followed by 30 minutes incubation to allow for CMFDA incorporation. Single cells were collected by trypsinizing the cells from the plate, quenching with trypsin inhibitor, washing with phosphate-buffered saline (PBS), fixing with 4% paraformaldehyde, and then quenching with glycine-containing PBS. Cells were subsequently stored in glycine-PBS until analysis.

Capillary electrophoresis separation of the content of a single cell was carried out in an uncoated fused silica capillary.[1,21] Single cell injection was performed by applying a 1s negative pressure at the sheath flow at the terminus of the capillary, causing siphoning and thus injection of a single cell, or a small volume of sample. Likewise, 2 plugs of triton X-100 were injected (before and after cell injection) to ensure lysis of the cell.

3. RESULTS AND DISCUSSION

Instrument performance

We first treat the signal to account for the photon counter's dead time;[13,22] we refer to data treated with this function as the corrected signal. To further increase the dynamic range of a capillary electrophoresis-laser induced fluorescence detector using CW excitation, we incorporated a series of beam-splitters into the fluorescence optical train. We scaled the data to correct for each diode's attenuation, and then combined the data to create a very wide dynamic range detector; this scaled data is presented in figure 2. In the full-scale data, Figure 2A, the most attenuated photodiodes' signals are used to present the major components in the electropherogram. The scaled peak amplitude, determined by scaling the signal from the most attenuated photodiode, is nearly 1 GHz. Figure 2B presents the signal at 100-fold higher sensitivity; the two major peaks show slight tailing, and a few trace impurities are visible. Figure 2C shows the signal at 10^4-fold higher sensitivity using the signal from the most sensitive photodiode. At this scale, tailing from the high-amplitude peaks extends across much of the electropherogram.

The origins of this tailing are not clear. This tailing could be caused by slow desorption from a small number of sites. This possibility is eliminated because the peak shape is preserved across at least five orders of magnitude in dye concentration (see figure S3 in supporting information). Saturation of the binding sites would lead to a nonlinear isotherm and variation in peak shape with concentration. The tailing also is not due to dead volume in the system, which would produce an exponentially-modified Gaussian peak shape; we fit the peaks with such a function, which failed to reproduce the tail. Finally, the tailing is not due to perturbation of the ionic strength by the sample; as shown below, such perturbations lead to peak fronting and only at much higher concentrations.

Part-per-billion impurities generate small peaks that rise above the tailing signal. In addition, a small offset that remains at the end of the electropherogram, which is likely due to minute amounts of sample that contaminate the running buffer vial. After injection, we rinse the tip of the capillary by dipping it in clean running buffer in a disposable centrifuge tube, and then discard the solution, which is replaced by fresh electrophoresis buffer in a new disposable centrifuge tube. Despite these precautions, it appears that a few parts per billion of solution made its way into the running buffer.

Calibration curve and dynamic range

Determining the linearity of wide dynamic range signals is not straightforward. With standards prepared by serial dilution, a simple plot of signal vs. concentration is virtually guaranteed to produce a high correlation linear plot. A more robust approach is to observe the slope of the calibration curve on log-log axes. If the signal increases linearly with concentration, the slope should be close to 1.0. Alternatively, the signal can be divided by analyte concentration. If the signal is linear, then the ratio is independent of concentration.

We constructed a calibration curve using dye concentrations from 5×10^{-12} M to 1×10^{-3} M. The main peak in the scaled electropherograms was fit with a Gaussian function and the peak areas are plotted in Figure 3. The slope of the log-log plot was 0.949 ± 0.003, $\chi_\nu^2=12$, across the billion-fold concentration range (from the 3 σ detection limit of 1 pM to 1 mM). As we show below, there is a systematic error at the highest concentration samples, presumably due to anti-stacking effects where the ionic strength due to the dye results in a decreased injection volume. Neglecting the two highest concentration samples, the slope of the log-log plot was 0.982 ± 0.007, $\chi_\nu^2=0.72$.

Figure 4 presents the signal divided by concentration. The ratio is nearly independent of concentration from 5×10^{-12} M to 1×10^{-5} M (slope = -0.125 ± 0.025). However, the ratio drops by roughly a factor of two for the 10^{-4} and 10^{-3} M solutions, reflecting the effect of the analyte's ionic strength on injection volume. We have normalized the Y-axis to the number of photons/molecule. For the domain where the injection volume appears to be well behaved, the weighted average signal was 3.1 photons/molecule.

Peak Shape at High Concentrations

We measured the number of theoretical plates for the major peak across the concentration range. The plate counts were constant at 900,000 ± 85,000 from 5×10^{-12} to 10^{-6} M, Figure 5. The plate counts decreased slightly at 10^{-5} μM and much more significantly at higher injected concentrations.

Figure 6A presents a close-up of the main peaks generated by the 10^{-3} M sample. The ionic strength of these components presumably perturbs the electric field in their vicinity, leading to peak distortion.[23] Such peak distortions lead to errors in calculation of peak moments.[24] In particular, peak height is underestimated and peak width is overestimated.

Figure 6B shows the profile of a trace impurity, which retains a Gaussian shape. The high ionic strength of the major components did not degrade the separation efficiency of the trace component; the unfiltered peak generated 750,000 theoretical plates.

Single cell analysis

We applied the very wide dynamic range instrument to the analysis of the metabolic products of single cells isolated from the rat cerebullum. Cultured cells were incubated with the fluorescence glycolipid GM1-TMR, which serves as a substrate for catabolism within the cell. Figure 7 presents electropherograms of the metabolic products from two single cells. The cultured cells include mainly neurons along with a small number of support cells isolated from the brains of young rats. Their diameters vary from 7 to 16 μm, which results in an order of magnitude difference in volume. Additional factors, such as cell type and cell age, apparently account for additional differences in the uptake and metabolism of the GM1 derivative.

Figure 8 presents the same data on a logarithmic intensity axis. The figure also presents identification of the major and minor components, as determined by comparison with the migration time of standard compounds. There is a remarkable difference in total signal, which reflects differences in uptake between the cells, and in the generation of *LacCer*, *GlcCer*, and the *Unknown* component, which reflects differences in metabolism between cells

4.0 Conclusion

We have demonstrated nine orders of magnitude dynamic range in capillary electrophoresis with laser induced fluorescence detection, and we have applied the instrument to metabolic cytometry of the metabolic contents of single primary neurons.

It is interesting to speculate on improvements to this instrument. Performance at higher concentrations is currently limited by electrophoretic peak distortion. While minor improvements are possible by use of higher ionic strength separation buffers, those improvements are limited. Significant improvements in dynamic range are only possible by improvement in detection limit, which is limited by noise in the background signal. One approach is to employ pulsed laser excitation and time-gated detection to discriminate against scattered laser photons.[25]

The ultimate performance would range from single molecule detection to electrophoretic saturation,[26] which would allow the widest possible dynamic range in electrophoretic detection—eleven or twelve orders of magnitude in analyte concentration should be possible. Application of this technology to metabolic cytometry will be fascinating; every product, down to the single molecule level, would be detected as long as the fluorescent tag remains intact in those products.[27]

Supplementary Material

Refer to Web version on PubMed Central for supplementary material.

Acknowledgments

This work was supported by grants IDBR 0963826 (NJD) from the National Science Foundation and R01NS061767 (NJD, OH, MMP, and RLS) from the National Institutes of Health.

Literature cited

1. Whitmore CD, Hindsgaul O, Palcic MM, Schnaar RL, Dovichi NJ. Anal. Chem. 2007; 79:5139–5142. [PubMed: 17567107]
2. Higuchi R, Fockler C, Dollinger G, Watson R. Biotechnology (N Y). 1993; 11:1026–1030. [PubMed: 7764001]
3. Russo-Marie F, Roederer M, Sager B, Herzenberg LA, Kaiser D. Proc. Natl. Acad. Sci. U S A. 1993; 90:8194–8198. [PubMed: 8396263]
4. Ramsay LM, Dickerson JA, Dada O, Dovichi NJ. Anal. Chem. 2009; 81:1741–1746. [PubMed: 19206532]
5. Kaye W. Anal. Chem. 1981; 53:369–374.
6. Dovichi NJ. TRAC, Trends Anal. Chem. (Pers. Ed.). 1984; 3:55–57.
7. Ingle JD, Crouch SR. Anal. Chem. 1972; 44:785–794.
8. Ingle JD, Crouch SR. Anal. Chem. 1972; 44:777–784.
9. Blackman M, Michiels JL. Proc. Phys. Soc. London. 1948; 60:549–561.
10. Sun XL, Davidson FM. J. Lightwave Techn. 1992; 10:1023–1032.
11. Gustafson TL, Lytle FE, Tobias RS. Rev. Sci. Instrum. 1978; 49:1549–1550. [PubMed: 18698999]
12. Kissick DJ, Muir RD, Simpson GJ. Anal. Chem. 2010; 82:10129–10134. [PubMed: 21114249]
13. Whitmore CD, Essaka D, Dovichi NJ. Talanta. 2009; 80:744–748. [PubMed: 19836546]
14. Dovichi NJ, Martin JC, Jett JH, Keller RA. Science. 1983; 219:845–847. [PubMed: 6823553]
15. Zhao JY, Chen DY, Dovichi NJ. J. Chromatogr. 1992; 608:117–120.
16. Cheng YF, Dovichi NJ. Science. 1988; 242:562–564. [PubMed: 3140381]
17. Wu SL, Dovichi NJ. J. Chromatogr. 1989; 480:141–155. [PubMed: 12408116]
18. Kraly JR, Jones MR, Gomez DG, Dickerson JA, Harwood MM, Eggertson M, Paulson TG, Sanchez CA, Odze R, Feng Z, Reid BJ, Dovichi NJ. Anal. Chem. 2006; 78:5977–5986. [PubMed: 16944874]
19. Mehta NR, Lopez PH, Vyas AA, Schnaar RL. J. Biol. Chem. 2007; 282:27875–27886. [PubMed: 17640868]
20. Larsson EA, Olsson U, Whitmore CD, Martins R, Tettamanti G, Schnaar RL, Dovichi NJ, Palcic MM, Hindsgaul O. Carbohydr. Res. 2007; 342:482–489. [PubMed: 17069778]
21. Whitmore CD, Olsson U, Larsson EA, Hindsgaul O, Palcic MM, Dovichi NJ. Electrophoresis. 2007; 28:3100–3104. [PubMed: 17668449]
22. Turner EH, Lauterbach K, Pugsley HR, Palmer VR, Dovichi NJ. Anal. Chem. 2007; 79:778–781. [PubMed: 17222051]
23. Gebauer P, Bocek P. Anal. Chem. 1997; 69:1557–1563.
24. McDowell LM, Barber WE, Carr PW. Anal. Chem. 1981; 53:1373–1376.

25. Harris JM, Chrisman RW, Lytle FE. Anal. Chem. 1976; 48:1937–1943.
26. Chen DY, Dovichi NJ. Anal. Chem. 1996; 68:690–696.
27. Hu K, Ahmadzadeh H, Krylov SN. Anal. Chem. 2004; 76:3864–3866. [PubMed: 15228369]

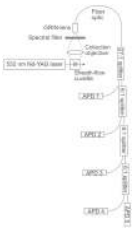

Figure 1.
Schematic diagram of the very wide dynamic range laser-induced fluorescence detector with a cascade of four fiber optics beam-splitters that divides the fluorescence signal into five channels, which are monitored by avalanche photodiodes. APD 1 provides the highest sensitivity but saturates at relatively low signal intensity. The beam-splitters successively present attenuated signals to the other APDs. APD 5 monitors the most attenuated signal.

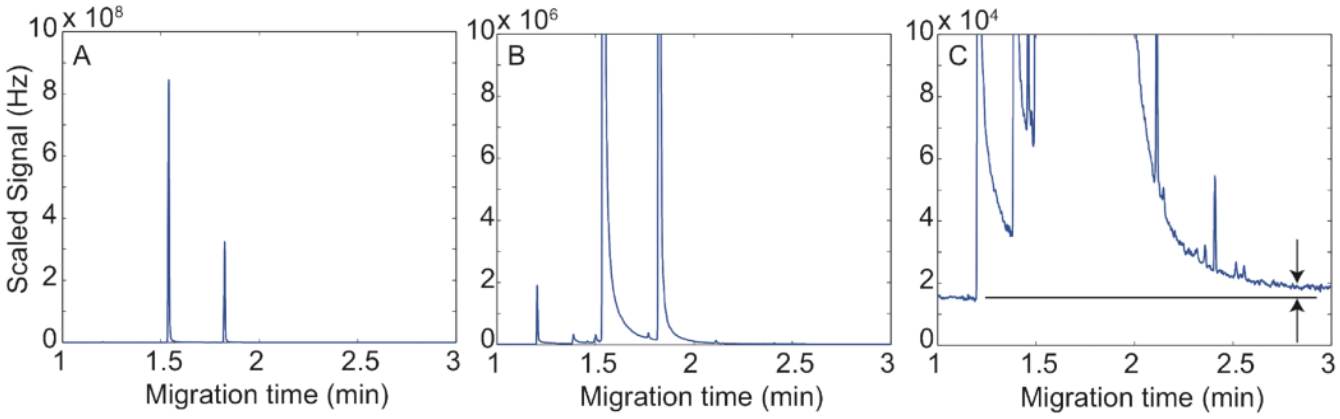

Figure 2.

Corrected and scaled electropherogram of 1 μM solution of TAMRA recorded with five photodiodes. The signals from APD 2, APD 3, APD 4, and APD 5 have been scaled to account for attenuation by the fiber optic beam-splitters and combined to create a single, very high dynamic range electropherogram. Panel A – The full scale data. Only the signals from the two main peaks are observed. Panel B – Expansion of the y-axis by two orders of magnitude to reveal minor components. Panel C – Expansion of the y-axis by two more orders of magnitude to reveal trace components. A minute offset due to buffer contamination is noted by the arrows. Another version of this figure is shown as Figure S1 in the supporting information for this paper; that version presents the Y-axis on a logarithmic scale. The corrected signals from the individual diodes are shown in Figure S2.

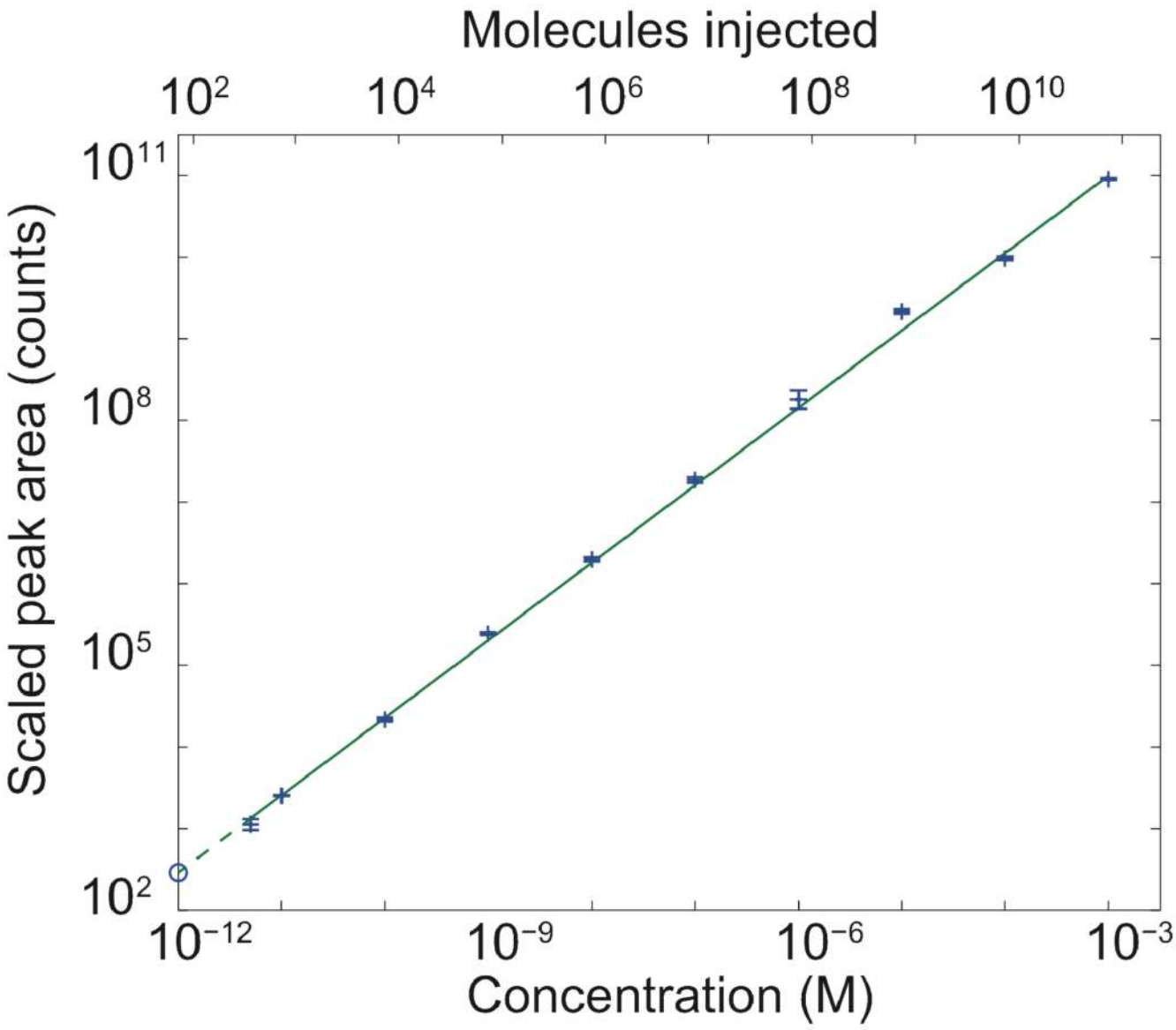

Figure 3.

Log-log calibration curve. Data are plotted ± one standard deviation of the mean. The straight line is a weighted least-squares fit to the log-log data. The 3 σ detection limit (1 pM) is plotted as the open circle and the extrapolation of the calibration curve to the detection limit is shown as the dashed line. As we show below, the highest concentration samples deviate slightly from the line because the ionic strength of the sample reduces the injection volume compared to lower concentrations. The upper axis provides an estimate of the number of molecules injected.

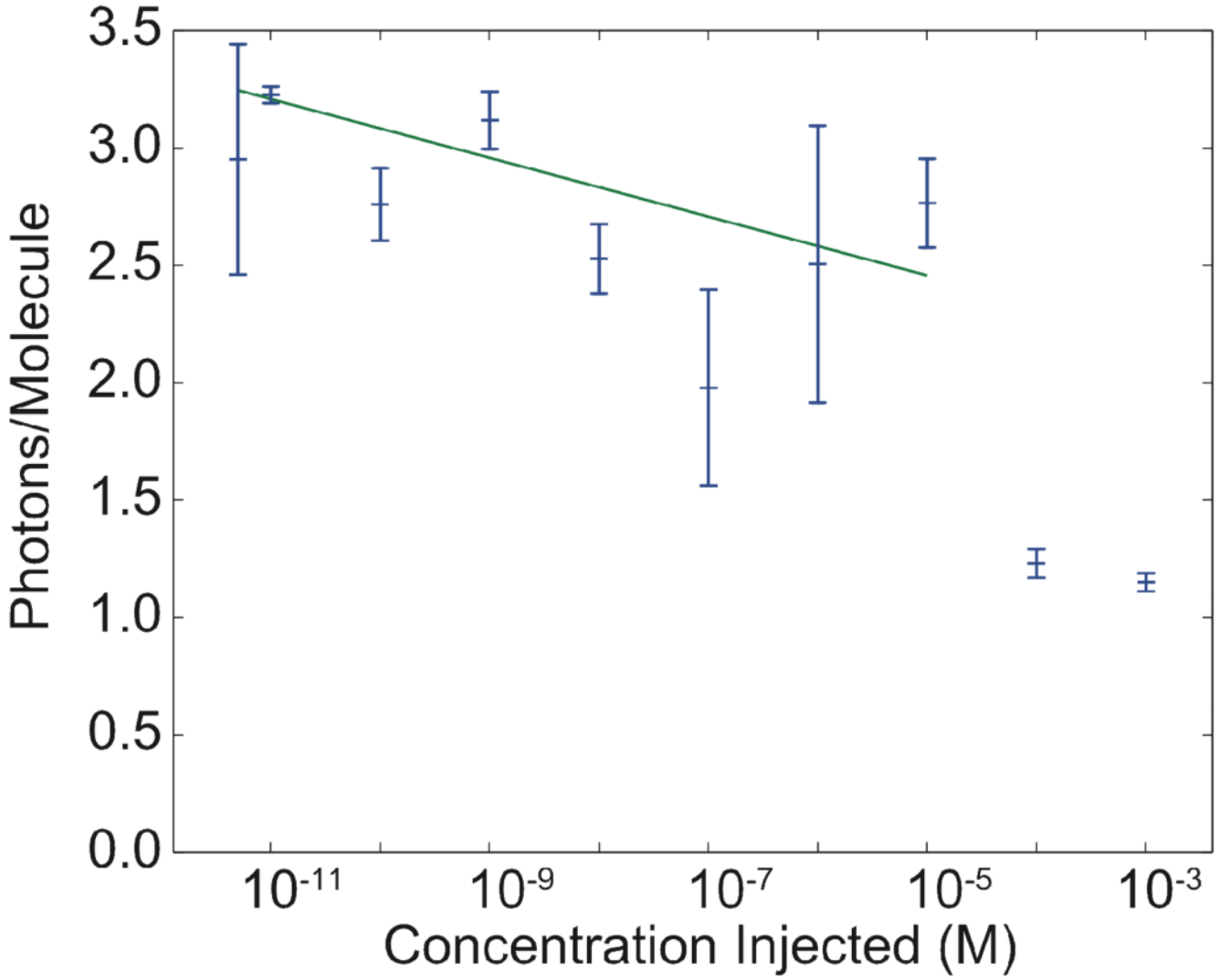

Figure 4.
Plot of the number of photons detected per molecule across the sample concentration range. The straight line is a weighted least squares fit of a line to the logarithm of concentration in the range of 5 pM to 100 μM. Data are plotted as ± one standard deviation of the mean.

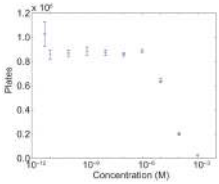

Figure 5.
Number of theoretical plates measured as a function of analyte concentration. Plates counts were determined by fitting a Gaussian function to the unprocessed peaks. Data are plotted as ± one standard deviation of the mean.

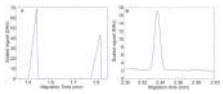

Figure 6.
Peak shape for 10^{-3} M sample. Panel A – Major components show fronting. Panel B – Trace component generates a Gaussian peak.

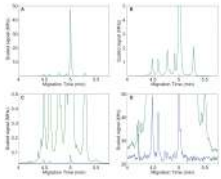

Figure 7.
Scaled electropherogram of two cerebellar granule neurons incubated with GM1 - TMR. One cell generated an intense signal (green trace) while the other generated a much weaker signal (blue trace). Panel A – Full-scale data. Panel B – Expansion highlights intermediate amplitude components of the intense cell. Panel C – Further expansion highlights trace components in the intense cell and major components in the weak cell. Panel D – Further expansion highlights ultratrace components in the intense cell and minor components in the weak cell.

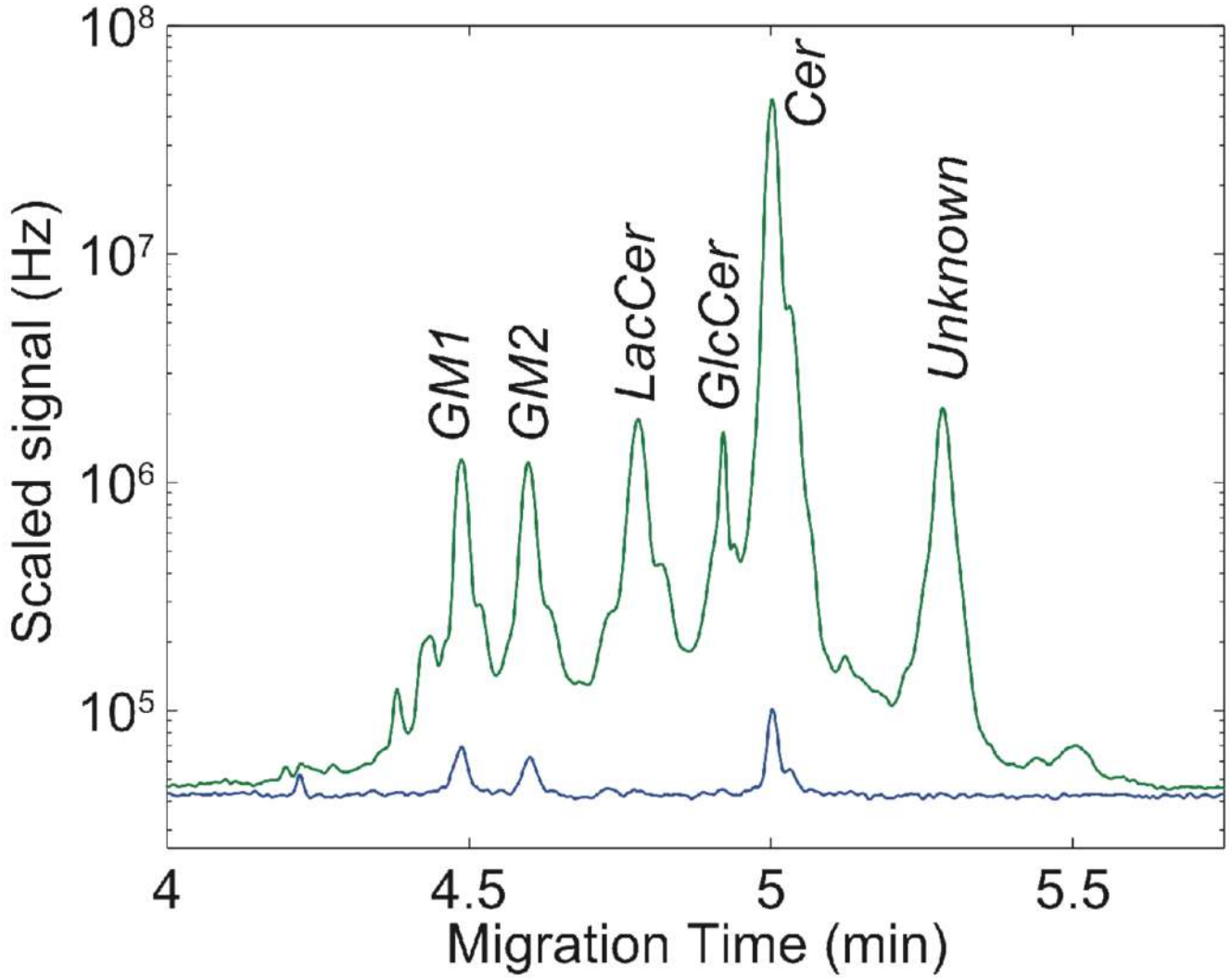

Figure 8.
Logarithmic Y-axis version of figure 7. The peaks are labeled based on the migration time of standards.